

A new metric for automatic discovery of periodic patterns in time series

Sayani Gupta *

Department of Econometrics and Business Statistics, Monash University, Australia
and

Rob J Hyndman

Department of Econometrics and Business Statistics, Monash University, Australia
and

Dianne Cook

Department of Econometrics and Business Statistics, Monash University, Australia

March 11, 2021

Abstract

Periodic patterns or associations in large univariate time series data could be discerned by analysing the behaviour across cyclic temporal granularities, which are temporal deconstructions accounting for repetitive behaviour. The temporal granularities form ordered categorical variables and display of distributions of the univariate response variable across two or more combinations of these categorical variable can help explore periodicities, patterns and anomalies. A pair of granularities that can be meaningfully examined together are called “harmonies” and the ones which cannot be are called “clashes”. Even after excluding clashes, the list of harmonies that could potentially be displayed is huge and hence overwhelming for human consumption. This work provides a methodology to screen the most informative graphics from the plethora of choices by introducing a distance measure that could be compared across harmonies with varied levels and data sets. Moreover, this distance measure could also be used to rank the selected harmonies basis how well they capture the variation in the measured variable. All the methods are implemented in the open source R package `hakear`.

Keywords: data visualization, periodicities, time granularities, cyclic granularities, permutation tests, Jensen-Shannon distances, smart meter data, R

*Email: Sayani.Gupta@monash.edu

1 Introduction

Exploratory data analysis, as coined by John W. Tukey (Tukey 1965) involves many iterations of finding structures and patterns that allow the data to be informative. With temporal data available at finer scales, exploring periodicity and their relationships can become overwhelming with so many possible cyclic temporal granularities (Gupta et al. 2020) to explore. Take the example of the calendar display of electricity smart meter data in Figure (1) used in Wang et al. (2020a) for four households in Melbourne, Australia. The authors show how hour-of-the-day interact with weekdays and weekends and then move on to use calendar display to show daily schedules. The calendar display has several components in it, which helps us to look at energy consumption across hour-of-the-day, day-of-the-week, week-of-the-month, and month-of-the-year at once. Some interaction of these cyclic granularities, for example, how day-of-week relates to month-of-year, could also be interpreted from this display. This is a great way for having an overview of energy consumption. However, if one wants to understand the periodicities in energy behavior and how the periodicities interact in greater detail, it is not easy to comprehend the interactions of some periodicities’ from this display, due to the combination of linear and cyclic representation of time. For example, this display might not be the best to understand how hour-of-the-day or month-of-year varies across week-of-the-month as well as with each other. Furthermore, it is not clear what all interactions of cyclic granularities should be read from this display as there could be many combinations that one can look at. Moreover, “*calendar effects are not restricted to conventional day-of-week or month-of-year deconstructions*” (Gupta et al. (2020)) and could include other cyclic granularities like hour-of-week or day-of-fortnight, which could potentially become useful depending on the context. Possible areas where it is useful are monitoring heart rates which could record number of heartbeats every minute or analyze web search data for which data is available for a temporal scale as fine as second.

Even when it is known which all interactions to look at, all of them would not be interesting and that too will vary across different households. For example, area distribution quantiles are plotted for household 2 and 4 in Figure 2a and 2b respectively across month-of-year on facets and hour-of-day on x-axis. For the first household, the 75th and 90th percentile for January and February are very close, implying that energy usage for these months are generally on a much higher side, possibly due to the usage of air conditioners (January and February are peak

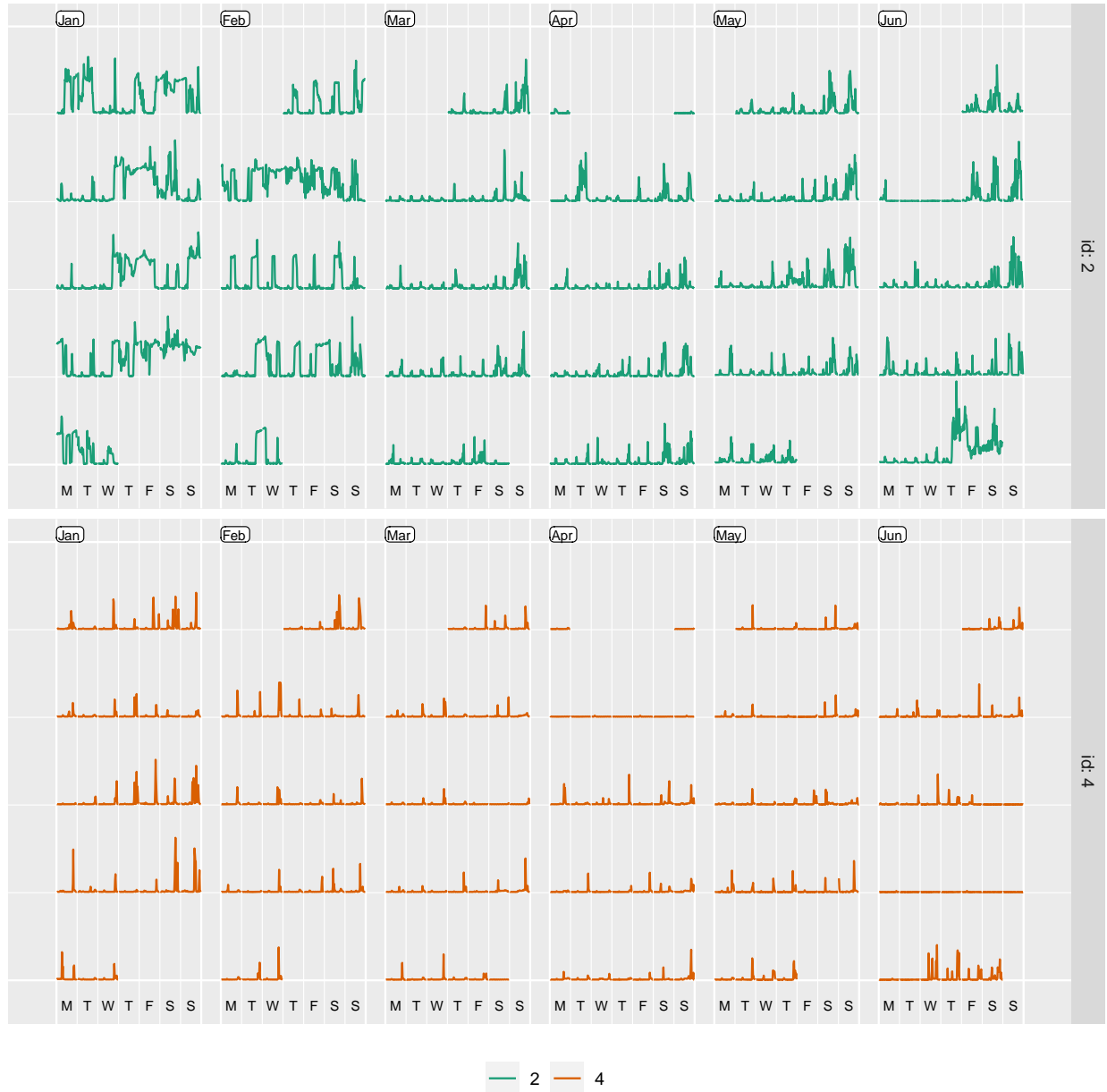


Figure 1: Calendar displays faceted by two households are shown. The calendar displays are rich in information and has several components. For example, it can be observed easily that the level of energy consumption by household 2 is higher than household 4. Also, it gives an overview on when these households are away for holidays and which months consumptions are highest (Jan, Feb). However, when it comes to discerning periodic patterns, analyzing all possible periodic patterns through this display is overwhelming due to combination of linear and cyclic representation of time. For example, there is more going on in terms of peaks and troughs in id 2 compared to id 4, but it is not clear which all periodic patterns are dominant and if it differs between households.

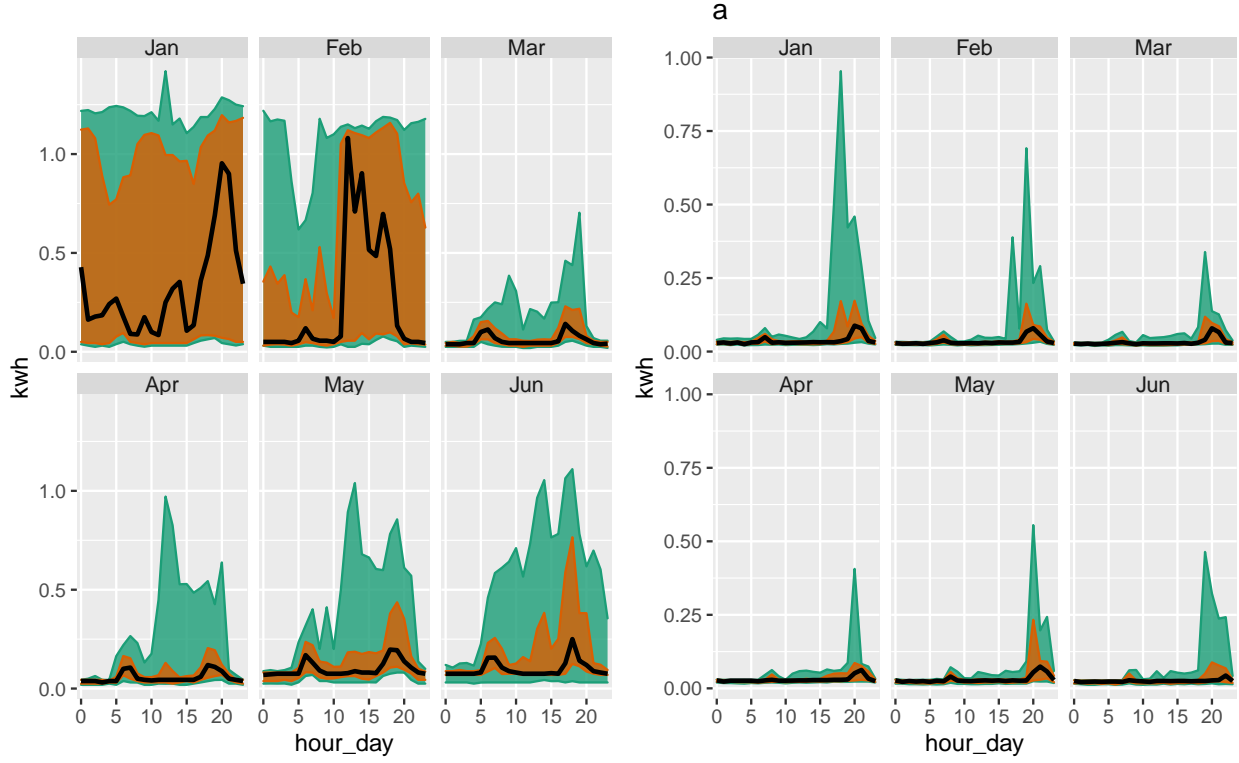


Figure 2: *Distribution of energy consumption displayed through area quantile plots across two cyclic granularities month-of-year and hour-of-day for id2 (left) and id4 (right). The black line is the median, whereas the orange band covers the 25th to 75th percentile and the green band covers the 10th to 90th percentile. Difference between the 90th and 75th quantiles is less for (Jan, Feb) in id2 suggesting that it is a more frequent user of air conditioner than id4. Energy consumption for id2 changes across both granularities, whereas for id4 daily pattern stays same irrespective of the months.*

summer in Australia), however for other months (Autumn and winter), the difference between the percentiles are not high, implying this household do not use so much heater as compared to air conditioner. Also, a lot of households in Victoria use gas heating and hence the usage of heaters might not be reflected here. The energy consumption for household 2 is also higher in summer months relative to autumn or winter, but the 75th and 90th percentile are far apart in all months, implying that the second household resorts to air conditioners much less regularly than the first one. Moreover, the 75th percentile distribution does not follow the same pattern as 90th percentile for all months for the first household, whereas, the pattern looks pretty similar for all months for the second household. Difference in the energy consumption could vary both across month-of-year (facets) and hour-of-day (x-axis). For the first household, both these cyclic granularities would deem important. Although, it seems like energy consumption across hours of the day are not that different across different months for the second household or atleast differences seem to be more prominent across month-of-year (facets) than hour-of-day (x-axis). It could be immensely useful to make the transition from all possible ways to only ways that could potentially be informative.

The paper Gupta et al. (2020) describes how we can compute all possible combinations of cyclic time granularities. Let N_C be the total number of contextual circular, quasi-circular and aperiodic cyclic granularities that can originate from the underlying linear granularities. The graphical mapping is such that distributions of a numeric response variable is displayed across combinations of cyclic granularities, one placed at x-axis and the other on the facet. That essentially implies there are ${}^{N_C}P_2$ possible pairwise plots exhaustively, where each plot would display a pair of cyclic granularities. This is large and overwhelming for human consumption. This problem is similar to Scagnostics (Scatterplot Diagnostics) by Tukey & Tukey (1988), which is used to discern meaningful patterns in large collections of scatterplots. Given a set of v variables, there are $v(v-1)/2$ pairs of variables, and thus the same number of possible pairwise scatterplots. Therefore, even for small v , the number of scatterplots can be large, and scatterplot matrices (SPLoMs) could easily run out of pixels when presenting high-dimensional data. Dang & Wilkinson (2014) and Wilkinson et al. (2005) provides potential solutions to this, where few characterizations help us to locate anomalies in density, shape, trend, and other features in the 2D point scatters.

This work is a natural extension of our work (Gupta et al. (2020)), which narrows down the search from ${}^{N_c}P_2$ plots by identifying pairs of granularities that can be meaningfully examined together (a “harmony”), or when they cannot (a “clash”). However, even after excluding clashes, the list of harmonies left could be enormous for exhaustive exploration. Hence, there is a need to reduce the search even further by including only those harmonies which are informative enough. Buja et al. (2009) and Majumder et al. (2013) present some methods to quantify the strength of pattern and noise through visual inference, similar to numerical testing. But this is an evolving field as human cognition (which act as the statistical tests in visual inference) might vary across humans even for the same plots. In this paper, we build a new distance measure which could be used to detect automatically detect significant periodic patterns.

Our contributions in this paper are:

- introduce a new distance measure for quantifying periodic interactions, which allows for identification of patterns in the time series data;
- devise a framework for choosing a threshold, which results in detection of only significantly interesting periodic patterns;
- show that the proposed distance metric could be used to rank the periodic patterns based on how well they capture the variation in the measured variable since they have been normalized for relevant parameters.

The article is organized as follows. Section 2 introduces a new distance measure, discusses the reasoning behind choosing such a measure and presents some results to study the behavior of the measure. Section 3 describes a methodology to normalize the distance measure so that it can qualify as a measure that can be compared across different comparisons and datasets. Section 4 discusses how to choose a threshold to select only significant harmonies. Section 5 presents an application to a residential smart meter data in Melbourne to show how this distance measure acts as a way to automatically detect periodic patterns in time series.

2 A distance measure for quantifying patterns in harmonies

We are interested in assessing the structure of the measured variable across bivariate cyclic granularities. We propose a measure called Weighted Maximum Pairwise Distances (wpd) to quantify

the structure in such a design. The principle employed towards this goal is explained through a simple example explained in Figure 3. Each of these figures have the same panel design with 2 x-axis categories and 3 facet levels. Figure 3a has all x categories drawn from $N(5, 10)$ distribution for each facet. It is not an interesting display particularly, as distributions do not vary across x-axis or facet categories. Figure 3b has x categories drawn from the same distribution within a facet but the mean has been incremented by 5 units for every consecutive facets. Figure 3c exhibits an exact opposite situation where distribution between the x-axis categories within each facet is different but they are same across facets. For this situation, mean of only the x-axis categories are increased by 5 units for each consecutive category. Figure 3d takes a step further by varying the distribution across both facet and x-axis categories. If the displays are to be ranked in order of importance from minimum to maximum, then an obvious choice would be placing a followed by b, c and then d. It might be argued that it is not clear if b should precede or succeed c in the ranking. Gestalt theory suggests that when items are placed in close proximity, people assume that they are in the same group because they are close to one another and apart from other groups. Hence, displays that capture more variation within different categories in the same group would be important to bring out different patterns of the data. With this principle in mind, display b is considered less informative as compared to display c. Hence, with reference to the graphical design in Gupta et al. (2020), therefore the idea would be to rate a harmony pair higher if the variation between different levels of the x-axis variable is higher on an average across all levels of the facet variables.

Intuitively, while finding a structure or measuring the strength of patterns in Figure 3, it makes sense to look for within-group and between-group variations. Larger variation would imply stronger patterns, whereas small variation would imply the underlying structure is not changing within or between group. Thus, a distance measure aimed to capture this structure should ideally estimate these within-group and between-group variations. One of the potential ways to do this is to measure the distances between distributions of the continuous random variable measured within and between groups, weigh them basis if they are within or between groups and then take the maximum of those distances as an estimate of the maximum variation in the structure. This section starts with possible ways of characterizing distributions and computing distances between them and then describe in details how the measure *wpd* is defined. This is similar to

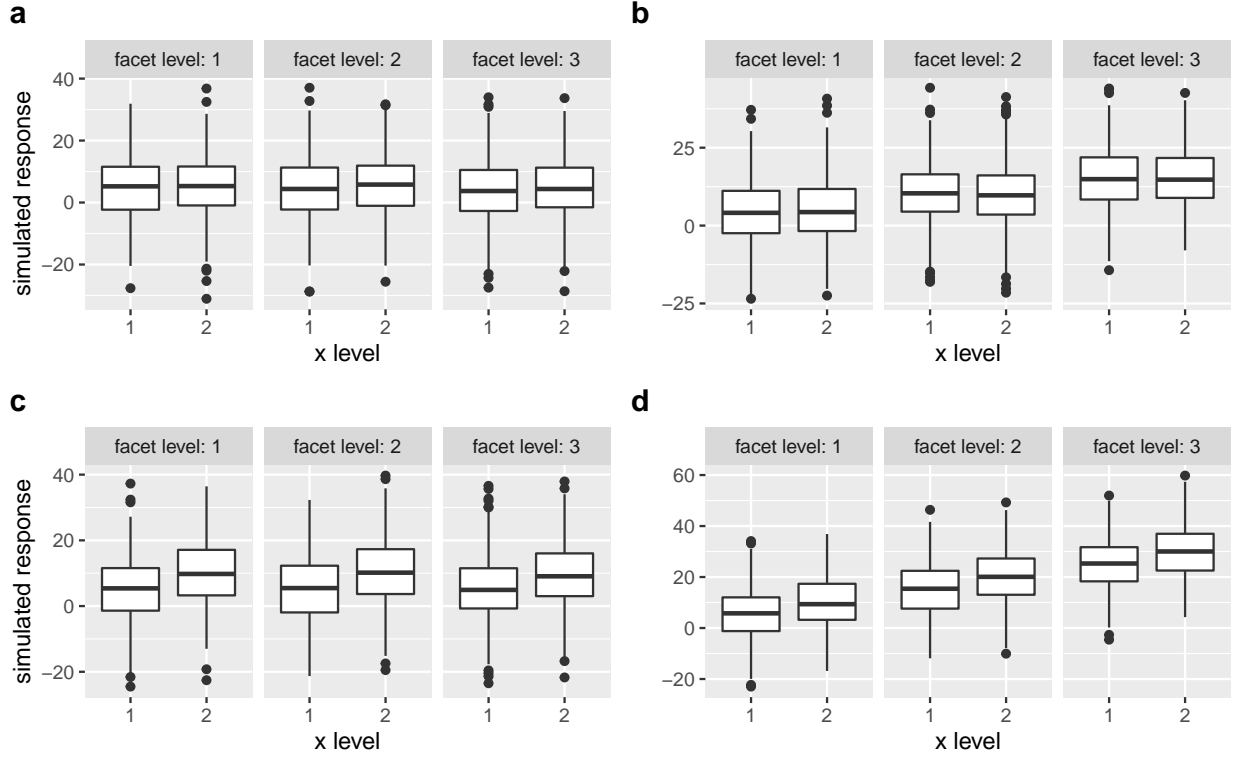


Figure 3: A graphical display with two categories mapped to x-axis and 3 categories mapped to facets with the distribution of a continuous random variable plotted on the y-axis. Display a is not interesting as the distribution of the variable does not depend on x or facet categories. Display b and c are more interesting than a since there is a change in distribution either across facets (b) or x-axis (c). Display d is most interesting in terms of displaying the strongest pattern as distribution of the variable changes across both facet and x-axis variable.

Hyndman et al. (2018) where the authors compute the Jensen Shannon distance between two density estimates by computing percentiles and stresses the advantages to working with percentiles rather than the raw data directly in case of missing observations. Working with quantiles also ensure that unsynchronized time series could be handled.

2.1 Notations

Consider two cyclic granularities A and B , such that $A = \{a_j : j = 1, 2, \dots, J\}$ and $B = \{b_k : k = 1, 2, \dots, K\}$ with A placed across x-axis and B across facets. Let $v = \{v_t : t = 0, 1, 2, \dots, T - 1\}$ be

a continuous variable observed across T time points. Let the four elementary designs as described in Figure 3 be D_{null} where there is no difference in distribution of v for A or B , D_{var_f} denotes the set of designs where there is difference in distribution of v for B and not for A . Similarly, D_{var_x} denotes the set of designs where difference is observed only across A . Finally, $D_{var_{all}}$ denotes those designs for which difference is observed across both A and B .

Table 1: *Nomenclature table*

variable	description
nx	number of x categories
$nfacet$	number of facet categories
N_C	number of cyclic granularities
H_{N_C}	set of harmonies
$lambda$	tuning parameter
$omega$	mean increment
wpd	raw distance measure
$nperm$	number of permutations for threshold/normalization
$nsim$	number of simulations
wpd_{norm}	normalized distance measure
$wpd_{threshold}$	threshold for significance
D_{null}	null design
D_{var_f}	design with varying facets only
D_{var_x}	design with varying x only
$D_{var_{all}}$	design with varying both facets and x

2.2 Characterising distributions

Multiple observations of v correspond to the subset $v_{jk} = \{s : A(s) = j, B(s) = k\}$. The number of observations and the structure might vary widely across subsets due to the structure of the calendar, missing observations or uneven locations of events in the time domain. Each v_{jk} 's $\forall j \in \{1, 2, \dots, J\}, k \in \{1, 2, \dots, K\}$ are assumed to be drawn from a continuous probability dis-

tribution and have certain characteristics. Often shape, central tendency, and variability are the common characteristics used to describe a distribution. Mean, median or mode are generally used to describe the center of the distribution, while range, standard deviation, quantiles, standard errors and confidence intervals are used to describe variability. Quantiles are chosen as a way to characterize distributions in this paper.

The quantile of a distribution with probability p is defined as $Q(p) = F^{-1}(p) = \inf\{x : F(x) > p\}$, $0 < p < 1$ where $F(x)$ is the distribution function. There are two broad approaches to quantile estimation, viz, parametric and non-parametric. The benefit of using a non-parametric estimator is that there are less rigid assumptions made about the nature of the underlying distribution of the data. Sample quantiles could be used for estimating population quantiles in a non-parametric setup. Hyndman & Fan (1996) describes the many ways of defining sample quantiles and recommends the use of median-unbiased estimator because of *desirable properties of a quantile estimator and can be defined independently of the underlying distribution..* The `stats::quantile()` function in R Core Team (2019) could be used for practical implementation where `type = 8` refers to the algorithm corresponding to the median-unbiased estimator. The default quantile chosen in this paper is percentiles computed for $p = 0.01, 0.02, \dots, 0.99$, where for example, the 99th percentile would be the value corresponding to $p = 0.99$ and hence 99% of the observations would lie below that.

2.3 Distance between distributions

The most common divergence measure between distributions is the Kullback-Leibler (KL) divergence (Kullback & Leibler 1951) introduced by Solomon Kullback and Richard Leibler in 1951. The KL divergence denoted by $D(q_1||q_2)$ is a non-symmetric measure of the difference between two probability distributions q_1 and q_2 and is interpreted as the amount of information lost when q_2 is used to approximate q_1 . Although the KL divergence measures the “distance” between two distributions, it is not a distance measure since it is not symmetric and does not satisfy the triangle inequality. The Jensen-Shannon divergence (Menéndez et al. 1997) based on the Kullback-Leibler divergence is symmetric and it always has a finite value. The square root of the Jensen-Shannon divergence is a metric, often referred to as Jensen-Shannon distance. Other common measures of distance between distributions are Hellinger distance, total variation

distance and Fisher information metric.

In this paper, we propose to use the pairwise distances between the distributions of the measured variable through Jensen-Shannon distance (JSD), defined by,

$$JSD(q_1||q_2) = \frac{1}{2}D(q_1||M) + \frac{1}{2}D(q_2||M)$$

where $M = \frac{q_1+q_2}{2}$ and $D(q_1||q_2) := \int_{-\infty}^{\infty} q_1(x)f(\frac{q_1(x)}{q_2(x)})$ is the KL divergence between distributions q_1 and q_2 .

Furthermore, these distances are distributed as chi-squared with m degrees of freedom (Menéndez et al. (1997)), if the continuous distribution is being discretized with m discrete values. Taking sample percentiles to approximate the integral would mean taking $m = 99$. As the degrees of freedom m get larger, the chi-square distribution approaches the normal distribution.

2.4 Computation

The distance measure *wpd* between two cyclic granularities A and B is aimed to capture the strength of the structure by estimating the maximum within-group and between-group variations. Furthermore, the intended aim of *wpd* is to capture differences in categories irrespective of the distribution from which the data is generated. Hence, as a pre-processing step, the raw data is normal quantile transformed (Bogner et al. (2012)) so that the quantiles of the transformed data follows a standard normal distribution. The steps employed for computing the distance measure is summarized as follows:

1. Perform NQT on the measured variable v_t to obtain v_t^* .
2. Fix harmony pair (A, B) .
3. Percentiles of v_{jk}^* are computed and stored in q_{jk} . Repeat for all pairs of categories of the form $(a_j b_k, a_{j'} b_{k'}) : \{a_j : j = 1, 2, \dots, J\}, B = \{b_k : k = 1, 2, \dots, K\}$.
4. The pairwise distances between pairs $(a_j b_k, a_{j'} b_{k'})$ denoted by $d_{(jk, j'k')} = JSD(q_{jk}, q_{j'k'})$ is computed.
5. The pairwise distances $d_{(jk, j'k')}$ is transformed using a suitable tuning parameter ($0 < \lambda < 1$) depending on if they are within-facet(d_w) or between-facets(d_b) as follows:

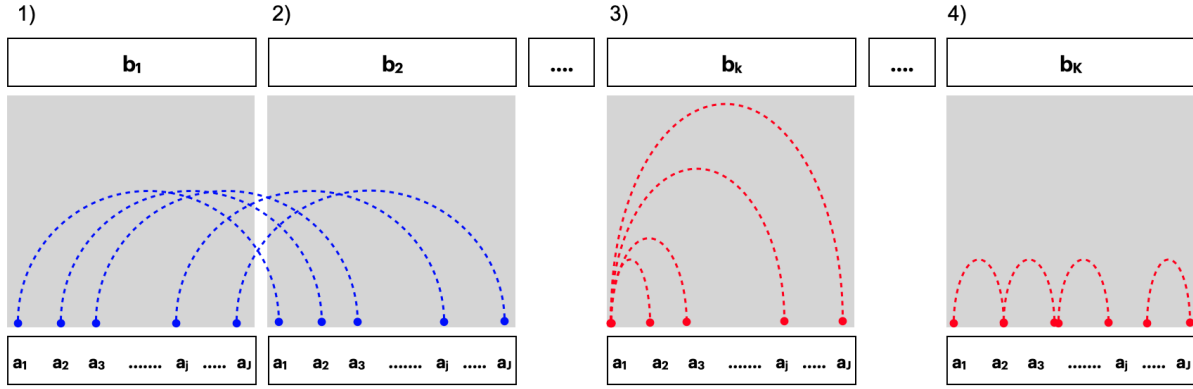


Figure 4: Within and between-facet distances shown for two cyclic granularities A and B , where A is mapped to x -axis and B is mapped to facets. The dotted lines represent the distances between different categories. Panel 1) and 2) show the between-facet distances. Panel 3) and 4) are used to illustrate within-facet distances when categories are unordered or ordered respectively. When categories are ordered, distances should only be considered for consecutive x -axis categories. Between-facet distances are distances between different facet levels for the same x -axis category, for example, distances between (a_1, b_1) and (a_1, b_2) or (a_1, b_1) and (a_1, b_3) .

$$d^*_{(j,k),(j',k')} = \begin{cases} \lambda d_{(jk),(j'k')}, & \text{if } d = d_w \\ (1 - \lambda) d_{(jk),(j'k')}, & \text{if } d = d_b \end{cases} \quad (1)$$

5. The wpd is then computed as $wpd = \max_{j,j',k,k'} (d^*_{(jk),(j'k')}) \forall j, j' \in \{1, 2, \dots, J\}, k, k' \in \{1, 2, \dots, K\}$.
6. Repeat Steps 2-5 for all harmony pairs in H_{N_C} .

Pairwise distances could be within-facets or between-facets. Figure 4 illustrates how the within-facet or between-facet distances are defined. Pairwise distances are within-facets when $b_k = b_{k'}$, that is, between pairs of the form $(a_j b_k, a_{j'} b_k)$ as shown in panel (3) of Figure 4. If categories are ordered (like all temporal cyclic granularities), then only distances between pairs where $a_{j'} = (a_{j+1})$ are considered (panel (4)). Pairwise distances are between-facets when they are considered between pairs of the form $(a_j b_k, a_{j'} b_{k'})$. Number of between-facet distances would be ${}^K C_2 * J$ and number of within-facet distances are $K * (J - 1)$ (ordered) and ${}^J C_2 * K$ (un-ordered). If the measure is intended to put more importance in pointing towards distributional differences between x categories, a $\lambda > 0.5$ should be chosen.

2.5 Properties

Simulations were carried out to explore the behavior of wpd under the following factors that could potentially impact the values of wpd : nx , $nfacet$, λ , ω , $dist$ (normal/non-normal distributions with different location and scale), $ntimes$, and $designs$ and results are presented in two parts. The dependence of wpd on nx and $nfacet$ under D_{null} is presented here, which lays the foundation for the next section. The rest of the results that discuss the relationship of the wpd with other factors is presented in details in the Supplementary section of the paper. They show that the designs D_{var_f} and D_{var_x} intersect at $\lambda = 0.5$ and hence for up-weighting designs of the form D_{var_x} , $\lambda = 0.67$ has been considered for computation of wpd in the rest of the paper.

2.5.1 Simulation design

Observations are generated from a Gamma(2,1) distribution for each combination of nx and $nfacet$ from the following sets: $nx = nfacet = \{2, 3, 5, 7, 14, 20, 31, 50\}$ to cover a wide range

of levels from very low to moderately high. Each combination is being referred to as a *panel*. That is, data is being generated for each of the panels $\{nx = 2, nfacet = 2\}, \{nx = 2, nfacet = 3\}, \{nx = 2, nfacet = 5\}, \dots, \{nx = 50, nfacet = 31\}, \{nx = 50, nfacet = 50\}$. For each of the 64 panels, $ntimes = 500$ observations are drawn for each combination of the categories. That is, if we consider the panel $\{nx = 2, nfacet = 2\}$, 500 observations are generated for each of the combination of categories from the panel, namely, $\{(1, 1), (1, 2), (2, 1), (2, 2)\}$. The values of wpd is obtained for each of the panels. This design corresponds to D_{null} as each combination of categories in a panel are drawn from the same distribution. Furthermore, the data is simulated for each of the panels $nsim = 200$ times, so that the distribution of wpd under D_{null} could be observed. $wpd_{l,s}$ denotes the value of wpd obtained for the l^{th} panel and s^{th} simulation.

2.5.2 Results

Figure 5 shows the distribution of wpd plotted across different nx and $nfacet$ categories. Since under D_{null} , there is no difference in distributions across different categories, we expect the distance measure wpd to reflect that as well and have the same distribution across categories. But Figure 5 shows that both the location and scale of the distributions change across panels. This is not desirable under D_{null} as it would mean comparisons of wpd values is not appropriate across different nx and $nfacet$. Figure 6 shows how the median of wpd varies with the total number of distances $nx * nfacet$ for each panel. The median increases abruptly for lower values of $nx * nfacet$ and slowly for higher $nx * nfacet$.

3 Normalization for the number of comparisons

The distribution of wpd is different for different levels of facets and x-axis levels. This is because the statistics maximum which is used to define wpd is affected by the number of comparisons (resulting pairwise distances). The measure would have higher values if A or B has higher levels. However, we would ideally want a higher value of the measure only if there are a significant difference between distributions across facet or x-axis categories, and not because the number of categories J or K is high. Therefore, in order to compare wpd across different combinations of facet and x-axis levels, we need to eliminate the impact of different number of comparisons

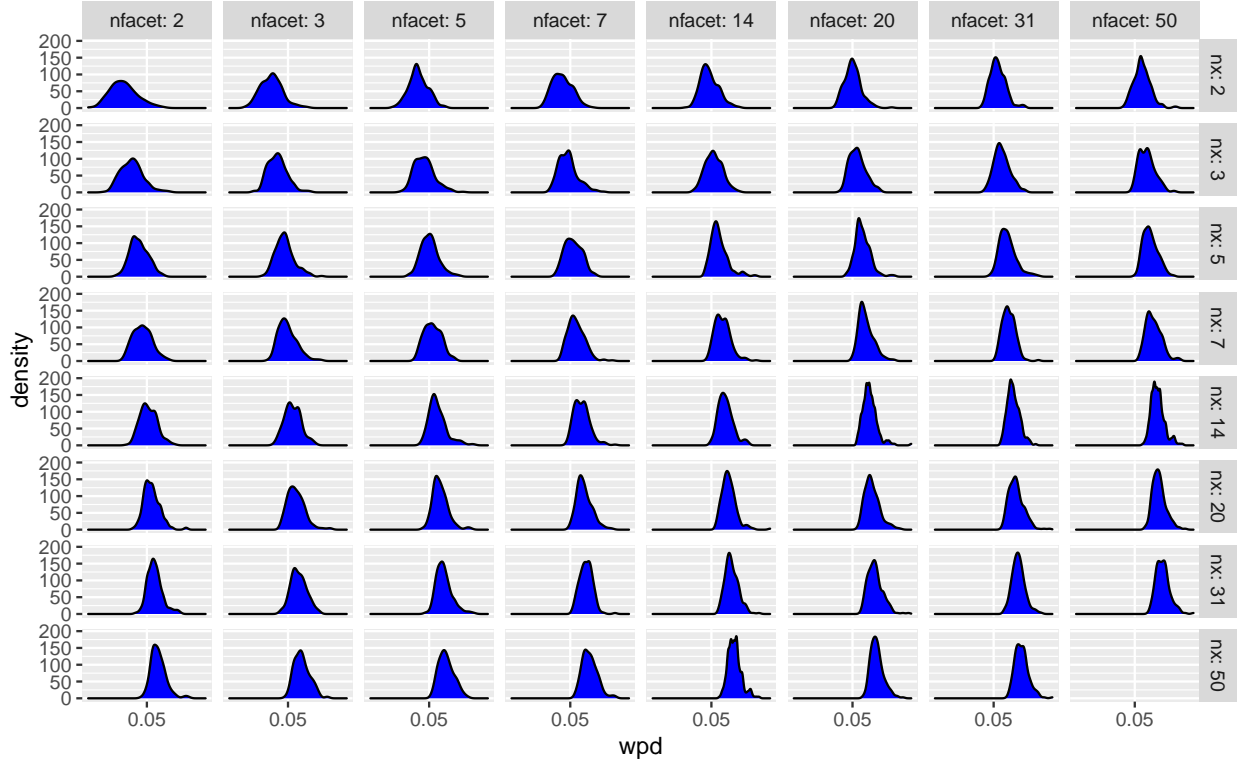


Figure 5: *Distribution of wpd is plotted across different n_x and n_{facet} categories under D_{null} . Both shape and scale of the distribution changes for different comparisons. This is not desirable since under null design, the distribution of the distance measure is not expected to capture any differences.*

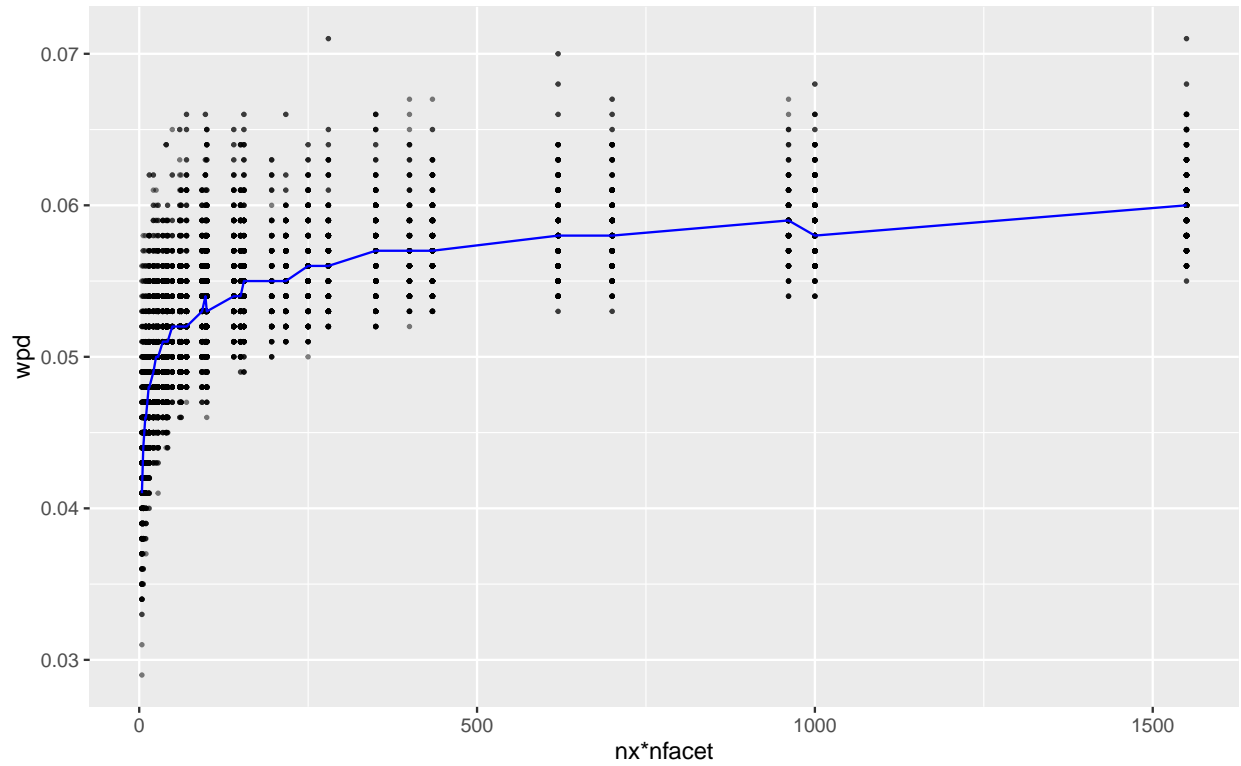


Figure 6: *wpd* is plotted against $nx * nfacet$ (the maximum number of pairwise comparisons) and the blue line represents the median of the multiple values for each $nx * nfacet$. The median increases abruptly for lower values of $nx * nfacet$ and slowly for higher $nx * nfacet$. Thus, the measure will have higher values for higher levels in nx or $nfacet$.

and get a normalized measure. Henceforth, we call the normalized measure as wpd_{norm} . The measure wpd_{norm} could potentially lead to comparison of the measure across different panels and also help distinguishing the interesting panels from a data set. We discuss two approaches for normalization, both of which are substantiated using simulations.

3.1 Methodology

The transformed wpd which is normalized for the values of nx and $nfacet$ is denoted by wpd_{norm} . Two approaches have been employed - the first one involves a permutation method to make the distribution of the transformed wpd similar for different comparisons and the second one fits a model to represent the relationship between the two variables and defines wpd_{norm} as the residual of the model.

3.1.1 Permutation approach

This method is somewhat similar in spirit to bootstrap or permutation tests, where the goal is to test the hypothesis that the groups under study have identical distributions. This method, in essence, accomplishes a different goal of making the location and scale of different groups (panels) same under D_{null} . The steps are as follows:

1. Compute wpd for a harmony pair (A, B) for the original measured variable v_t and store it in wpd_{orig} .
2. Consider a permutation of the original measured variable v_{perm_1} and again compute wpd for the permuted data. Store it in wpd_{perm_1} .
3. Repeat Step 2 for a large number ($nperm = 200$) of random permutations of the data yielding $nperm$ values : $wpd_{perm_1}, wpd_{perm_2}, \dots, wpd_{perm_{nperm}}$. Store the vector in wpd_{perm} .
4. Define $wpd_{perm} = \frac{(wpd_{orig} - \bar{wpd}_{perm})}{sd(wpd_{perm})}$, where \bar{wpd}_{perm} and $sd(wpd_{perm})$ are the mean and standard deviation of wpd_{perm} respectively.

Standardizing wpd in the permutation approach ensures that the distribution of wpd_{perm} has the same $mean = 0$ and $sd = 1$ across all comparisons under D_{null} . While this works successfully to make the location and scale similar across different nx and $nfacet$ (as seen in Figure 7), it is

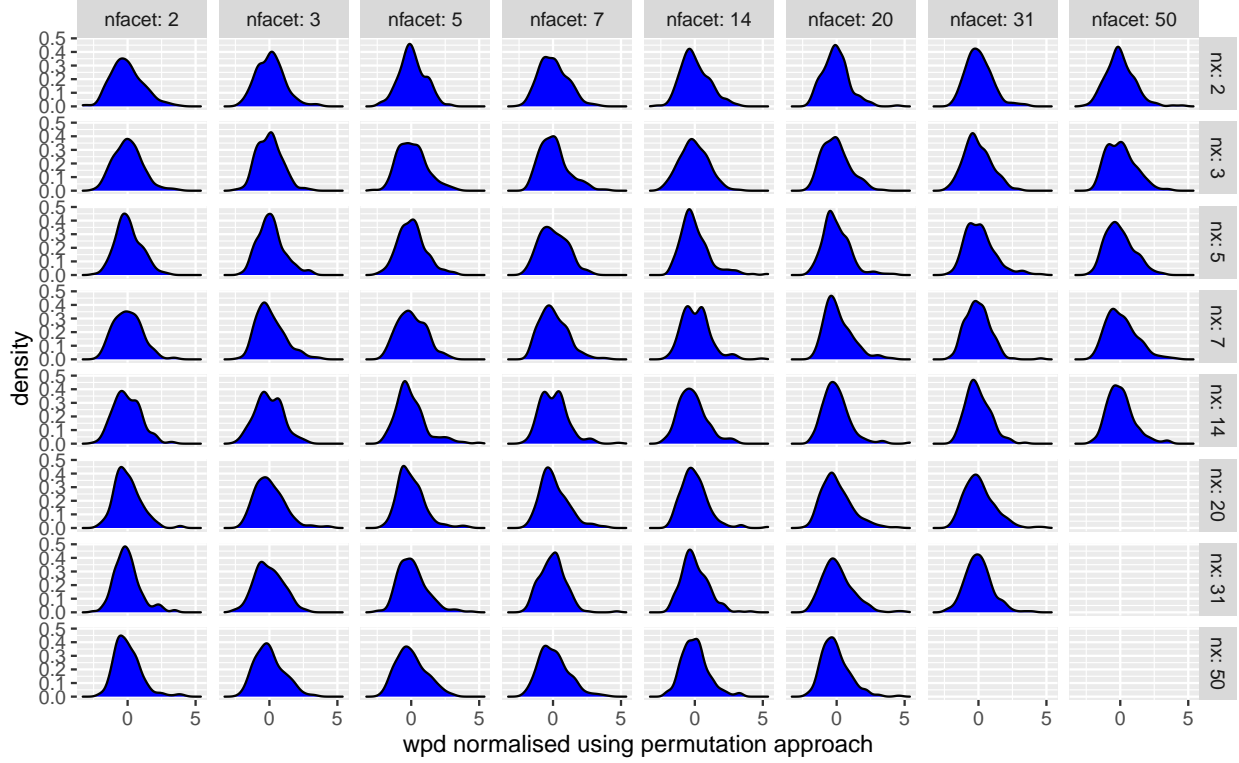


Figure 7: Distribution of wpd_{perm} is plotted across different nx and $nfacet$ categories. Both shape and scale of the distributions are now similar for different panels under the null design.

computationally heavy and time consuming, and hence less user friendly when being actually used in practice. Hence, we propose another approach to normalization which is more approximate than exact but still has the similar accuracy when compared to the permutation approach.

3.1.2 Modelling approach

Linear model

A linear model is fitted to model the relationship between wpd and $nx * nfacet$. The model is of the form

$$y_l = a + b * \log(z_l) + e_l$$

, where, $y_l = median_m(wpd_{l,m})$, z_l is the l^{th} panel and e_l are idiosyncratic errors, with parameters a and b being estimated from the data generated through the simulation study described in Section 2.5.1. The estimates and other model summary is given in Table 2.

Table 2: Results of linear model to capture the relationship between *wpd* and number of comparisons.

term	estimate	std.error	statistic	p.value
(Intercept)	0.0403697	0.0003814	105.85081	0
log('nx * nfacet')	0.0027565	0.0000804	34.27252	0

The idea is to find a transformation on *wpd* which would remove the effect of $nx * nfacet$ on *wpd* and thus is defined as the residuals: $y^* = y - \hat{a} - \hat{b} * \log(z)$, where y^* is the wpd_{linear} , \hat{a} and \hat{b} are the estimated values of the parameter a and b and $z = nx * nfacet$.

Defining wpd_{linear} in this way forces the mean to be zero and variability to be uniform across the median *wpd* values as could be seen in Figure 8.

Generalized linear model

In the linear model approach, $wpd \in R$ was assumed, whereas, *wpd* is a Jensen-Shannon Distance (JSD) and lies between 0 and 1 (Lin (1991)). Furthermore, JSD follows a Chi-square distribution, which is a special case of Gamma distribution. Therefore, a generalized linear model could be fitted instead of a linear model to allow for the response variable to follow a Gamma distribution. The inverse link is used when we know that the mean response is bounded, which is applicable in our case since $0 \leq wpd \leq 1$.

We fit a Gamma generalized linear model with the inverse link which is of the form:

$$y_l = a + b * \log(z_l) + e_l$$

, where $y_l = median_m(wpd_{l,m})$, z_l is the l^{th} panel and e_l are idiosyncratic errors. Let $E(y) = \mu$ and $a + b * \log(z) = g(\mu)$ where g is the link function. Then $g(\mu) = 1/\mu$ and $\hat{\mu} = 1/(\hat{a} + \hat{b} \log(z))$. The residuals from this model $(y - \hat{y}) = (y - 1/(\hat{a} + \hat{b} \log(z)))$ would be expected to have no dependency on z . Thus, wpd_{glm} is chosen as the residuals from this model and is defined as: $wpd_{glm} = wpd - 1/(\hat{a} + \hat{b} * \log(nx * nfacet))$.

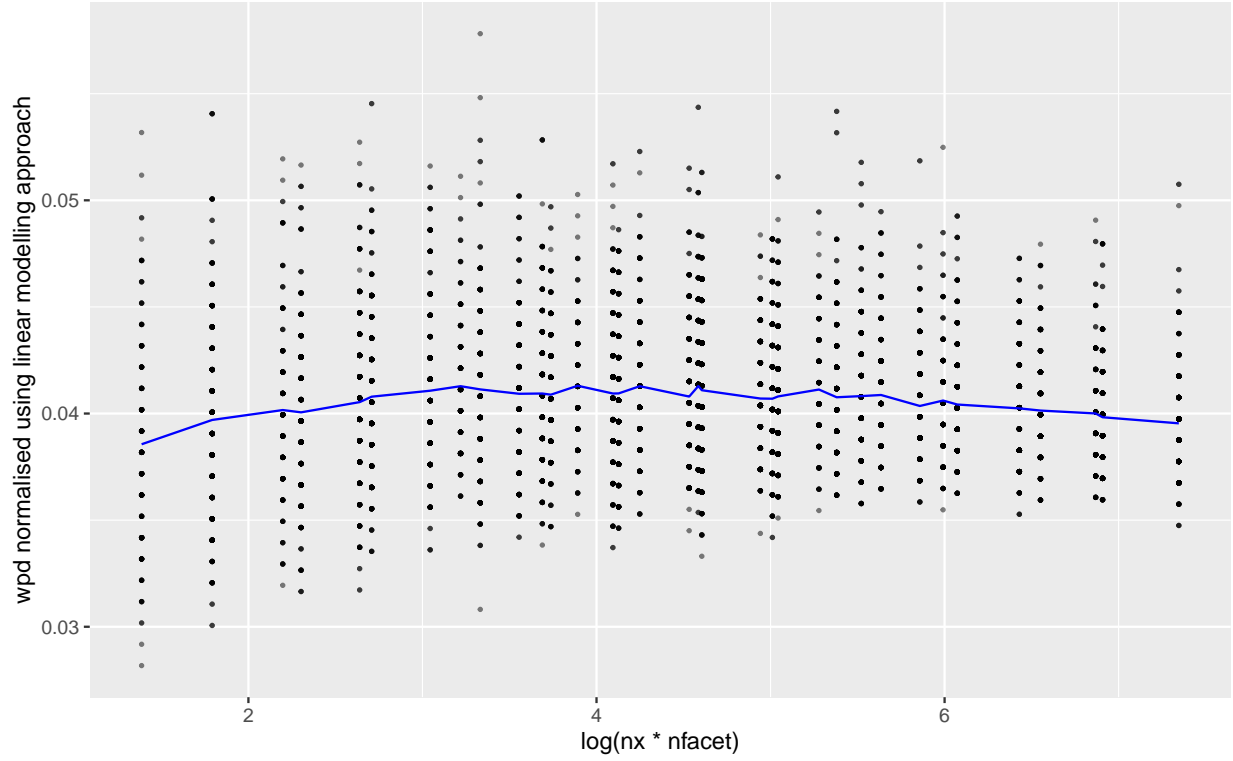
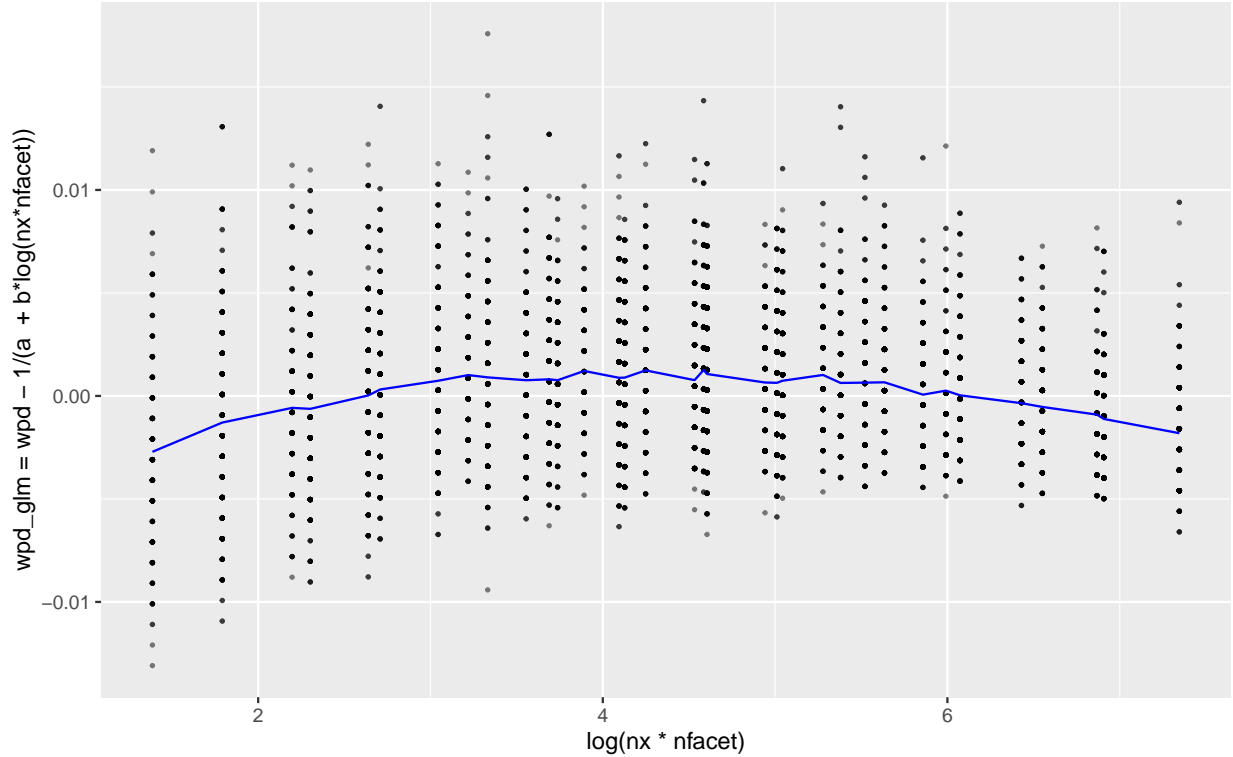


Figure 8: wpd_{norm}^{linear} which are defined as the residuals of the linear model have mean zero and are homogenous. Further, by design they are independent of the $nx * nfacet$ and hence could be a potential candidate for wpd_{norm} .

Table 3: Results of generalised linear model to capture the relationship between *wpd* and number of comparisons.

term	estimate	std.error	statistic	p.value
(Intercept)	23.5587633	0.2207781	106.7079	0
log('nx * nfacet')	-0.9971299	0.0444104	-22.4526	0



3.2 Combining normalizing approaches

We see that the transformation through the modeling approach leads to very similar distribution across high *nx* and *nfacet* (higher than 5) and not so much for lower *nx* and *nfacet*. Hence, the computational load of permutation approach could be alleviated by using the modeling approach for the higher *nx* and *nfacet*, however, it is important that we use the permutation approach for lower *nx* and *nfacet*. It is difficult to compare and use the transformed measure from both of these approaches alternatively without bringing them to the same scale. The transformed variables from the two approaches have to be brought to the same scale so that for smaller categories,

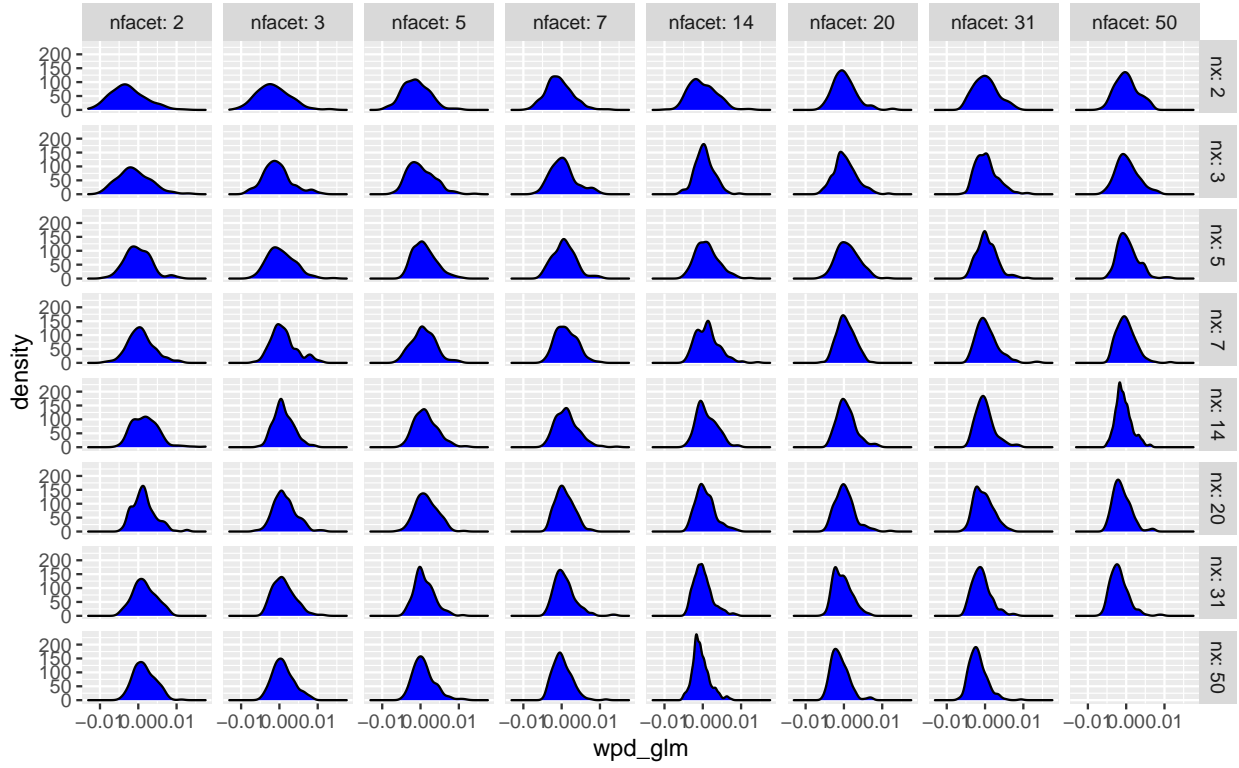


Figure 9: The distribution of wpd_{glm} is plotted. The distributions are more similar across higher nx and $nfacet$ and dissimilar for fewer nc and $nfacets$.

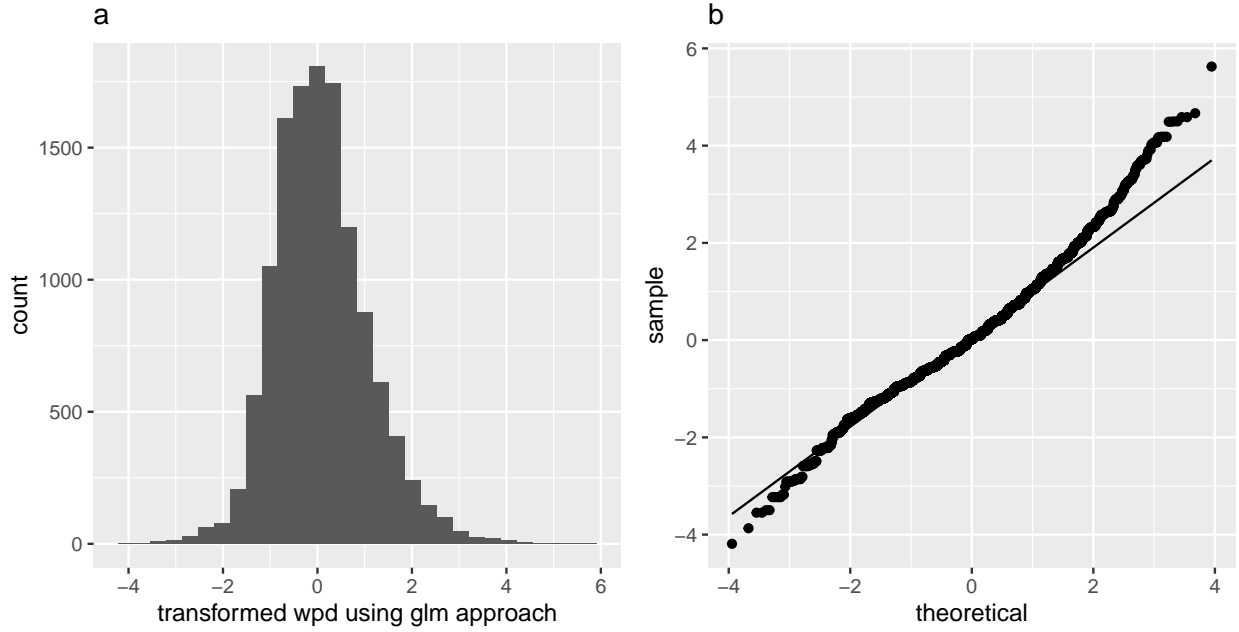


Figure 10: In panel a, the histogram of $wpd_{glm-scaled}$ is plotted. In part b, the QQ plot is shown with the theoretical quantiles on the x-axis and $wpd_{glm-scaled}$ quantiles on the y-axis. The distribution looks symmetric and looks like normal except in the tails.

permutation approach is used and for larger categories, modeling approach is used.

The measure wpd_{glm} has a $\hat{\mu}_{glm} = 0$ and $\hat{\sigma}_{glm} = 0.003$ whereas the measure wpd_{perm} which is a z-score, has an expected normal distribution with $\hat{\mu}_{perm} = 0$ and $\hat{\sigma}_{perm} = 1$. To bring them to the same scale, we have defined $wpd_{glm-scaled} = wpd_{glm} * \frac{\hat{\sigma}_{perm}}{\hat{\sigma}_{glm}}$, which changes the scale of wpd_{glm} without changing the location. The measure $wpd_{glm-scaled}$ seems to roughly follow a normal distribution except in the tails as could be seen in Figure 10 and the very method of permutation approach ensures that wpd_{perm} is also normally distributed. Further, they are brought to similar scale and location and hence could be compared or used interchangeably for different comparisons based on their performance.

Thus, the wpd_{norm} is defined as follows:

$$wpd_{norm} = \begin{cases} wpd_{perm}, & \text{if } J, K \leq 5 \\ wpd_{glm-scaled} & \text{otherwise} \end{cases} \quad (2)$$

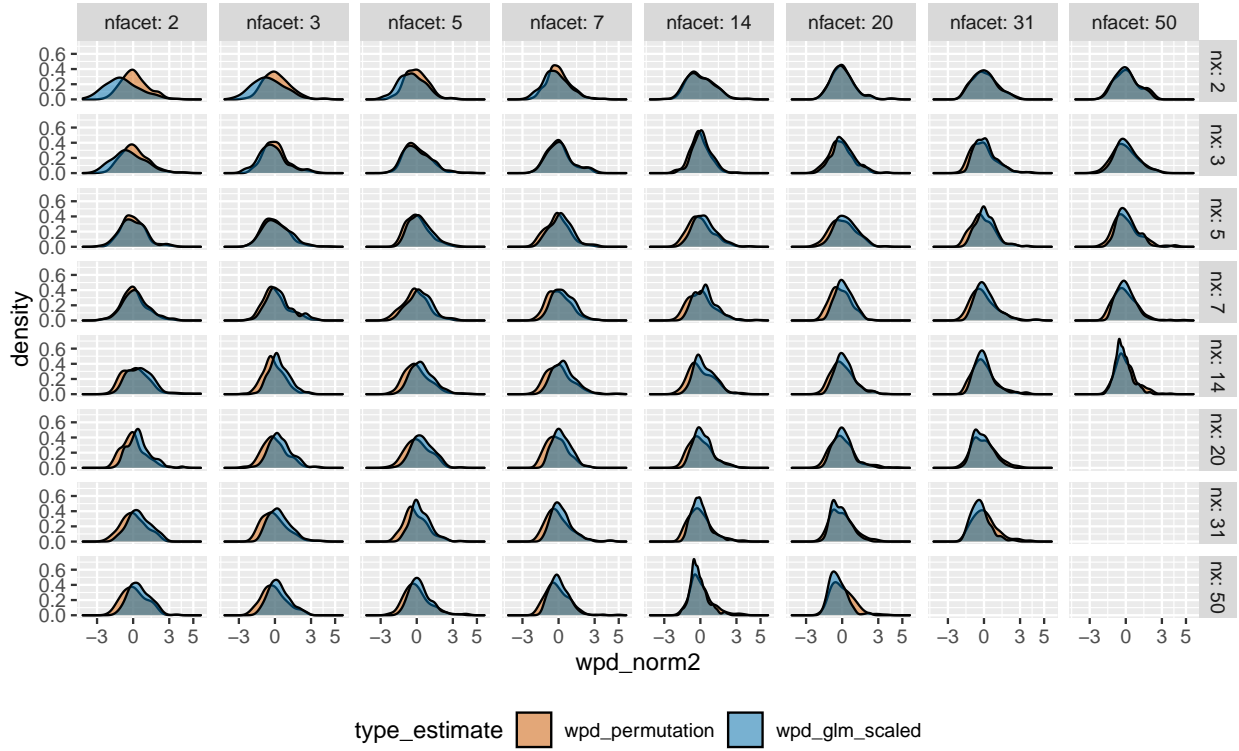


Figure 11: wpd_{perm} and $wpd_{glm-scaled}$ are plotted together on the same scale. They also have the same location and hence the values from these two approaches could be compared across panels. $wpd_{glm-scaled}$ would be used to normalise wpd_{raw} for higher n_x and n_{facet} and wpd_{perm} would be used for smaller levels to alleviate the problem of computational time.

3.3 Properties

This section reports the results of a simulation study that was carried out to evaluate the behavior of wpd_{norm} under different designs and other potential factors. The behavior of wpd_{norm} is explored in designs where there is in fact difference in distribution between facet categories (D_{var_f}) or across x-categories (D_{var_x}) or both ($D_{var_{all}}$). Using $\omega = \{1, 2, \dots, 10\}$ and $\lambda = seq(from = 0.1, to = 0.9, by = 0.05)$, observations are drawn from a $N(0,1)$ distribution for each combination of nx and $nfacet$ from the following sets: $nx = nfacet = \{2, 3, 5, 7, 14, 20, 31, 50\}$. $ntimes = 500$ is assumed for this setup as well. Furthermore, to generate different distributions across different combination of facet and x levels, the following method is deployed - suppose the distribution of the combination of first levels of x and $facet$ category is $N(\mu, \sigma)$ and μ_{jk} denotes the mean of the combination ($a_j b_k$), then $\mu_j = \mu + j\omega$ (for design D_{var_x}) and $\mu_k = \mu + k\omega$ (for design D_{var_f}).

The tabulated values and graphical representations of the simulation results are provided in the Supplementary paper. The learning from the simulations are as follows: The values of wpd_{norm} is least for D_{null} , followed by D_{var_f} , D_{var_x} and $D_{var_{all}}$. This is a desirable result since the measure wpd_{norm} was designed such that this relationship holds. Furthermore, the distribution of the measure wpd_{norm} does not change for different facet and x categories. The distribution of wpd_{norm} looks similar with at least the mean and standard of the distributions being uniform across panels. This means wpd_{norm} could be used to measure differences in distribution across panels. Also, note that since the data is processed using normal-quantile-transform, this measure is independent of the initial distribution of the underlying data and hence is also comparable across different data sets. This is valid for the case when sample size $ntimes$ for each combination of categories is at least 30 and $nperm$ used for computing wpd_{norm} is at least 100. More detailed results about the properties of wpd_{norm} could be found in the Supplementary paper.

4 Ranking and selecting significant harmonies

In this section, we provide a method to select important harmonies by eliminating all harmonies for which patterns are not significant by employing randomization test. Randomization tests (permutation tests) generates a random distribution by re-ordering our observed data and allow to test if the observed data is significantly different from any random distribution. Complete randomness

in the measured variable indicates that the process follows a homogeneous underlying distribution over the whole time series, which essentially implies there is no interesting distinction across any different categories of the cyclic granularities.

4.1 Choosing a threshold

A randomization test involves calculating a test statistic, randomly shuffling the data and calculating the test statistic several times to obtain a distribution of the test statistic. But we will use this procedure to obtain a threshold such that harmony pairs with a wpd_{norm} value higher than this threshold will only be considered significant. The process of choosing a threshold is described as follows:

- **Input:** All harmonies of the form $\{(A, B), A = \{a_j : j = 1, 2, \dots, J\}, B = \{b_k : k = 1, 2, \dots, K\}\}$ with A placed across x-axis and B across facets $\forall (A, B) \in N_C$.
 - **Output:** Harmony pairs (A, B) for which wpd_{norm} is significant.
1. Fix harmony pair (A, B) .
 2. Given the data; $\{v_t : t = 0, 1, 2, \dots, T - 1\}$, the wpd_{norm} is computed and is represented by wpd_{obs} .
 3. From the original sequence a random permutation is obtained: $\{v_t^* : t = 0, 1, 2, \dots, T - 1\}$.
 4. wpd_{norm} is computed for the permuted sequence of the data and is represented by wpd_{perm_1} .
 5. Steps (3) and (4) are repeated a large number of times M ($M = 200$).
 6. For each permutation, one wpd_{perm_i} is obtained. Define $wpd_{sample} = \{wpd_{perm_1}, wpd_{perm_2}, \dots, wpd_{perm_M}\}$.
 7. Repeat Steps (1-6) for all harmony pairs $(A, B) \in H_{N_C}$ and store it in wpd_{sample}^{all} .
 8. 99th percentiles of wpd_{sample}^{all} is computed and stored in $wpd_{threshold99}$.
 9. If $wpd_{obs_{A,B}} > wpd_{threshold99}$, harmony pair (A, B) is selected with a 99% level of significance and otherwise rejected.

Similarly, a harmony pair (A, B) is selected with a 95% and 90% level of significance if $wpd_{obs_{A,B}} > wpd_{threshold95}$ and $wpd_{obs_{A,B}} > wpd_{threshold90}$, where $wpd_{threshold95}$ and $wpd_{threshold90}$ denote the 95th and 90th percentile of wpd_{sample}^{all} respectively.

4.2 Simulation design

Observations are generated from a $N(0,1)$ distribution for each combination of nx and $nfacet$ from the following sets: $nx = \{3, 7, 14\}$ and $nfacet = \{2, 9, 10\}$. The panel $(3, 2), (7, 9), (14, 10)$ are considered to have design D_{null} . The panels $(7, 2), (14, 9)$ have design of the form D_{var_f} . $(14, 2), (3, 10)$ have design of the form D_{var_x} and the rest are under $D_{var_{null}}$. We generate only one data set for which all these designs were simulated and consider this as the original data set. We generate 200 repetitions of this experiment with different seeds and compute the proportion of times a panel is rejected when it is under D_{null} . We also compute the proportion of times a panel is rejected when it actually belongs to a non-null design. The first proportion is desired to be as small as possible and a higher value of the later is expected. Also, these would constitute to be the estimated size and power of the test.

4.2.1 Results

The results for this section is WIP and to be included in details in the Supplementary paper. Also, Figure 12 presents the results of wpd_{norm} from the illustrative designs in Section 2. As expected, the value of wpd_{norm} under null design is the least (a), followed by (b, c and d). Moreover, note the relative difference in wpd_{norm} values as we move from a to d, which aligns with the idea of wpd_{norm} , since the differences between x categories are up-weighted by design.

4.3 Simulation environment

Simulation studies were carried out to study the behavior of wpd , build the normalization method as well as compare and evaluate different normalization approaches. R version 4.0.1 (2020-06-06) is used with the platform: x86_64-apple-darwin17.0 (64-bit) running under: macOS Mojave 10.14.6 and MonaRCH, which is a next-generation HPC/HTC Cluster, designed from the ground up to address the computing needs of the Monash HPC community.

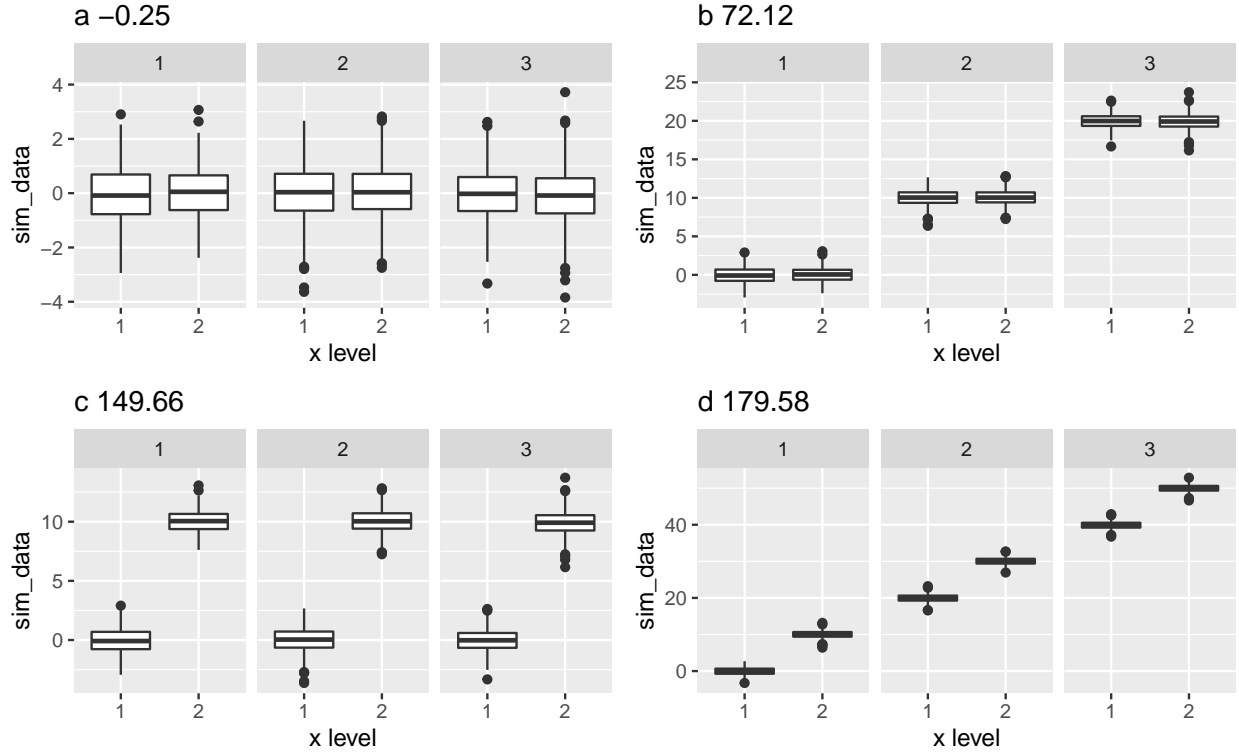


Figure 12: wpd_{norm} values for the four illustrative designs are presented here. As expected, the value of wpd_{norm} under null design is the least (a), followed by (b, c and d). Moreover, the relative difference is interesting as c is closer to d than b, since the differences between x categories are up-weighted by design.

5 Application to residential smart meter dataset

The smart meter data set for eight households in Melbourne has been utilized to see the use of wpd_{norm} proposed in the paper. The data has been cleaned to be a `tsibble` (Wang et al. (2020b)) containing half-hourly electricity consumption from Jul-2019 to Dec-2019 for each of the households, which is procured by them by downloading their data from the energy supplier/retailer. We also have some additional demographics data in terms of the number of members in the household and the presence of kids/elderly parents and their profession.

Demand data for these households are shown in a linear time scale in Figure 13. In the left panel of Figure 13 (a), the linear representation of the entire time period is shown, whereas in the right panel (b) a particular month is shown and furthermore a week has been highlighted. It is evident from the range of the demand data in Figure 13 (a), that these households vary in consumption levels, but all their periodic patterns have been squeezed with this representation. When we zoom into the linear representation of this series in Figure 13 (b), some patterns are visible in terms of peaks and troughs, but we do not know if they are regular or what is their period. Electricity demand, in general, has a daily and weekly periodic pattern. However, it is not apparent from this view if all of these households have those patterns and in case they have if they are significant enough. Also, it is not clear if any other periodic patterns are present in any household which might have been hidden with this view. We start the analysis by asking if the ranking of the harmonics make sense for the households, then compare households to get more insights of what these rankings imply and if they could be used to remove some non-interesting harmonics. Furthermore, we see if the display of the significant harmonics could be validated by zooming in the linear representation of the time series.

Table 4: *Demographics of the eight households chosen for study*

id	profession	total_members	kids	old_parents	PhD_student
1	academia	2	no	no	no
2	mixed	3	no	yes	yes
3	industry	5	yes	yes	no
4	industry	5	yes	yes	no
5	mixed	2	no	no	yes

id	profession	total_members	kids	old_parents	PhD_student
6	mixed	2	no	no	yes
7	academia	2	no	no	yes
8	industry	6	yes	yes	no

Choosing cyclic granularities of interest and removing clashes

Let $v_{i,t}$ denote the electricity demand for i^{th} household for time period t . The series $v_{i,t}$ is the linear granularity corresponding to half-hour since the interval of the tsibble is 30 minutes. We consider coarser linear granularities like hour, day, week and month from the commonly used Gregorian calendar. Considering 4 linear granularities hour, day, week, month in the hierarchy table, the number of cyclic granularities is $N_C = (4 * 3/2) = 6$. We obtain cyclic granularities namely “hour_day”, “hour_week”, “hour_month”, “day_week”, “day_month” and “week_month”, read as “hour of the day”, etc. Further, we add cyclic granularity day-type(“wknd wday”) to capture weekend and weekday behavior. Thus, 7 cyclic granularities are considered to be of interest. The set consisting of pairs of cyclic granularities (C_{N_C}) will have $7P_2 = 42$ elements which could be analyzed for detecting possible periodicities. The set of possible harmonies H_{N_C} from C_{N_C} are chosen by removing clashes using procedures described in (Gupta et al. 2020). Table 5 shows 14 harmony pairs that belong to H_{N_C} .

Selecting and Ranking harmonies for all households

$v_{i,t}$ has a asymmetrical distribution as could be seen in Figure 14 and the Normal score transform has been applied to make it more symmetric. Let $v^*_{i,t}$ denote the normal-quantile transformed electricity demand for i^{th} household for time period t . Suppose $(A, B) \in H_{N_C}$ be a harmony pair where $A = \{a_j : j = 1, 2, \dots, J\}$ and $B = \{b_k : k = 1, 2, \dots, K\}$ with A placed across x-axis and B across facets. Suppose $q_{A,j}^{i,p}$ denote the quantiles with probability p for the of the i^{th} household for j^{th} category of the cyclic granularity A . Similarly, $q_{B,k}^{i,p}$ denotes the same for the k^{th} category of the cyclic granularity B . Sample quantiles were computed at $p = 0.01, 0.02, \dots, 0.99$. Jensen-Shannon distances are computed between $q_{A,j}^{i,p}$ and $q_{B,k}^{i,p}$ for each $j \in J, k \in K$ to obtain the relevant within-facet and between-facet distances. A tuning parameter of $\lambda = 0.67$ has been considered in Equation 1 to compute wpd . It is further normalized using the approach described in Section 3. This entire process is repeated for all harmony pairs $\in H_{N_C}$ and for each households

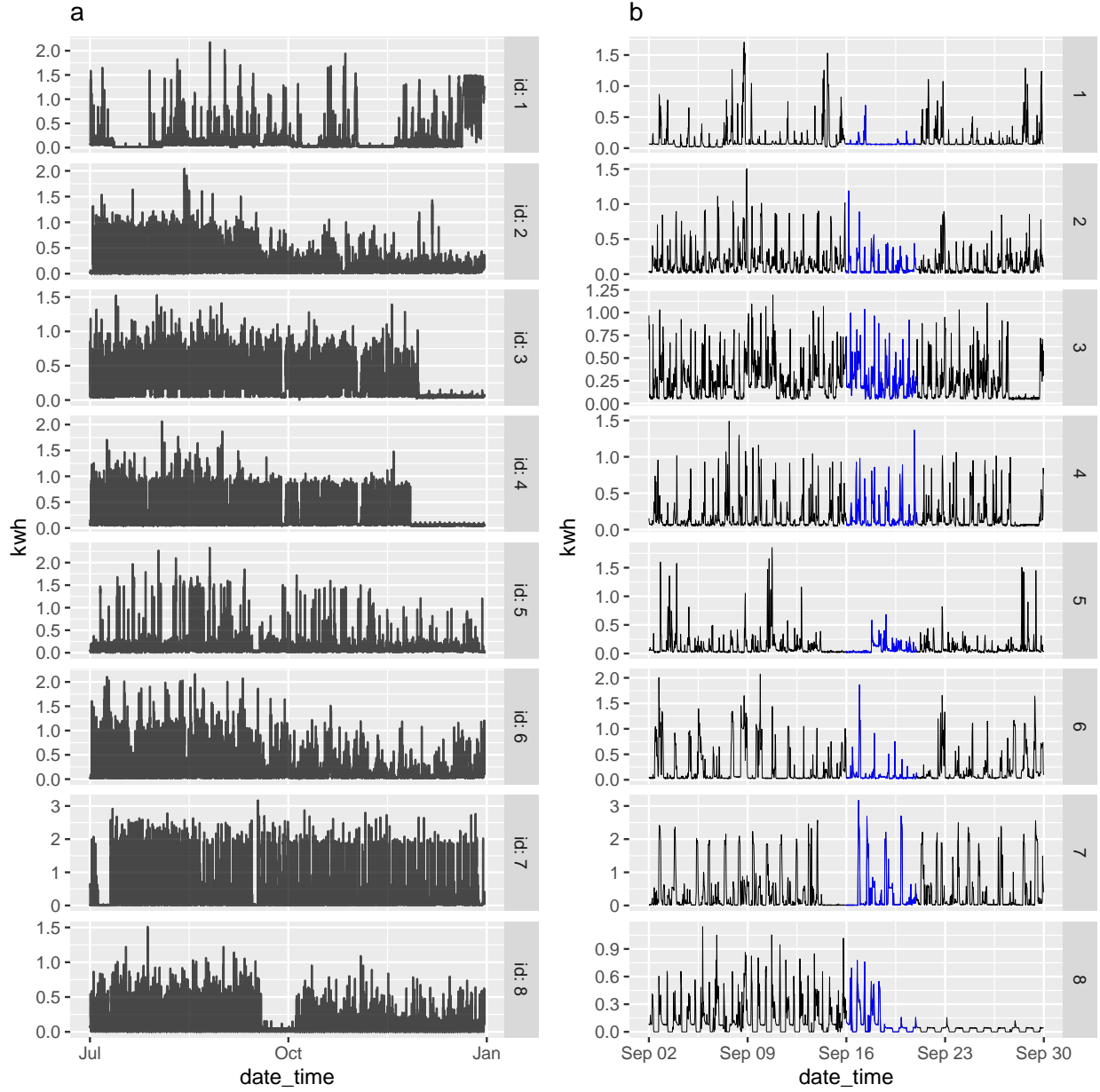


Figure 13: Electricity demand for eight households is shown in different facets from Jul-19 to Dec-19 in Fig a and it has been zoomed in for Sep-19 in Fig b, where a week in Sep-19 has been highlighted. From the scales of Fig a, it is apparent that these households vary in consumption levels, but all their periodic patterns have been squeezed with this representation. In fig b, we can see some weekly patterns for the entire period and daily patterns for the highlighted week and there could be some other patterns visible in terms of peaks and troughs, but it is not clear if they are regular or significant.

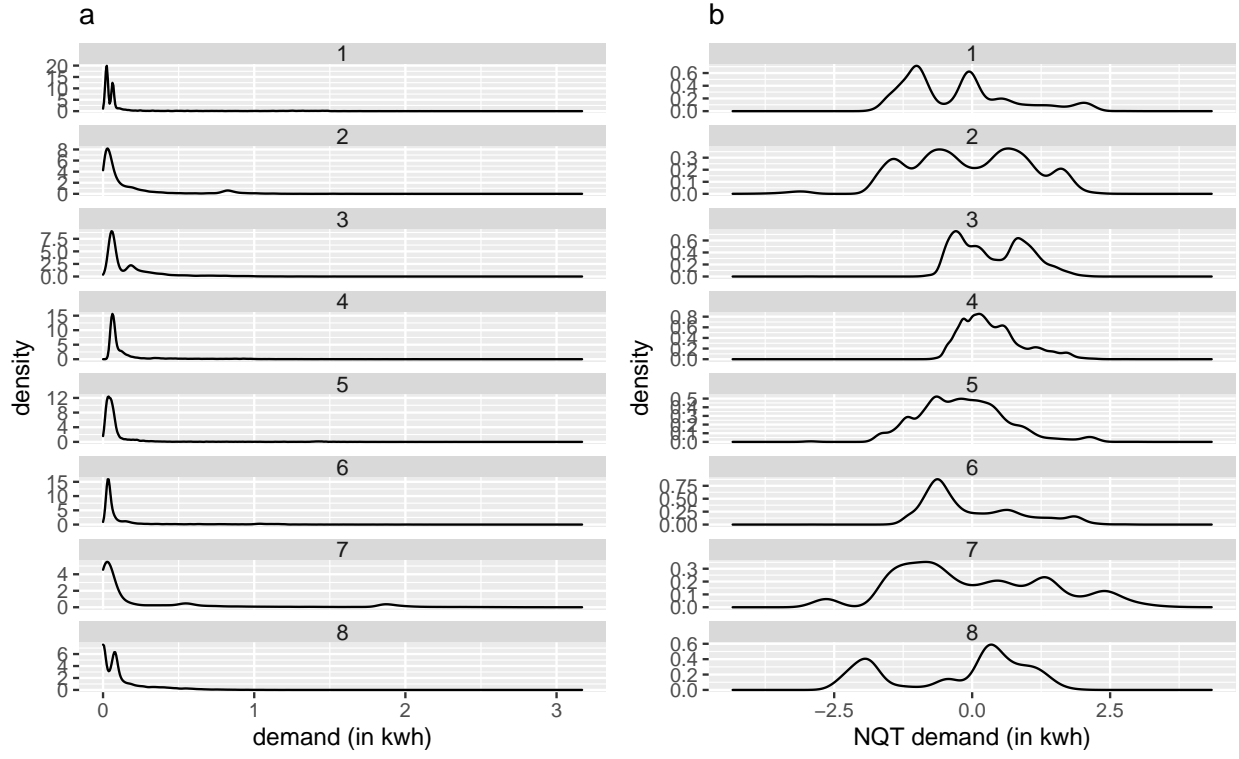


Figure 14: The raw density of the half-hourly demand for the eight households is shown in Fig a. Fig b shows the normal-score-transformed half-hourly demand for the same households which has resulted in more symmetric distribution of half-hourly demand.

$i \in i = \{1, 2, \dots, 8\}$. The harmony pairs are then arranged in descending order and the important ones with significance level 1%, 5% and 10% are highlighted with ***, ** and * respectively. Table 5 shows the rank of the harmonies for different households. Figure 16 shows the heatmap for the eight households with the value of wpd_{norm} filled as colors.

Validating rank of household id:1

From table 5, it could be seen that for household id:1, (hod, wdwnd) has been ranked higher than (wdwnd, hod), both of these being significant. Further, we see that (wom, wdwnd) has been ranked 5th and tagged as an insignificant pair. Figure 15 is used to show if this selection and ranking of harmony pairs makes sense for this household. Panel a) of Figure 15 shows the distribution of energy demand with weekday/weekend as the x-axis and hour-of-day as the facets and helps to compare the weekend/weekday patterns for different hours of the day. It could be observed that the difference between weekend and weekday is the highest from 15 to 19 hours of the day. Panel b) shows the distribution of energy demand with the variables swapped and helps to compare the daily patterns within weekday and weekend. It could be observed that the daily pattern is similar for weekdays and weekends with a morning and evening peak. However, the difference between morning and evening peaks are higher for weekends. Since wpd_{norm} is designed to put more weightage on within-facet differences for $\lambda > 0.5$, it makes sense that the pair (hod, wdwnd) has been ranked higher than (wdwnd, hod). Panel c) shows the distribution of energy demand with weekday/weekend as the x-axis and week-of-month as the facets. Although the differences might seem significant at first, with closer inspection it could be seen that the scale of the demand is lower in this case and hence the differences are not large enough to cross the threshold for significance.

Comparing households and validating patterns from linear display

Figure 16 helps to compare households through the heatmap (a) and validate the results of the heatmap through linear display in (b). The top panel contains the raw data for a month (Sep-2019). The darker the color of a cell in the heatmap, the more significant a harmony pair it is. Also, the ones with * are significant at 95% level. This plot suggests that there are no significant periodic patterns for id 5, even when the demographics of id 5 are very similar to id 6 and 7. Household id 6 and 7 differ in the sense that for id 6, the difference in patterns only during weekday/weekends (two members are in the mixed profession), whereas for id 7, all or few other days

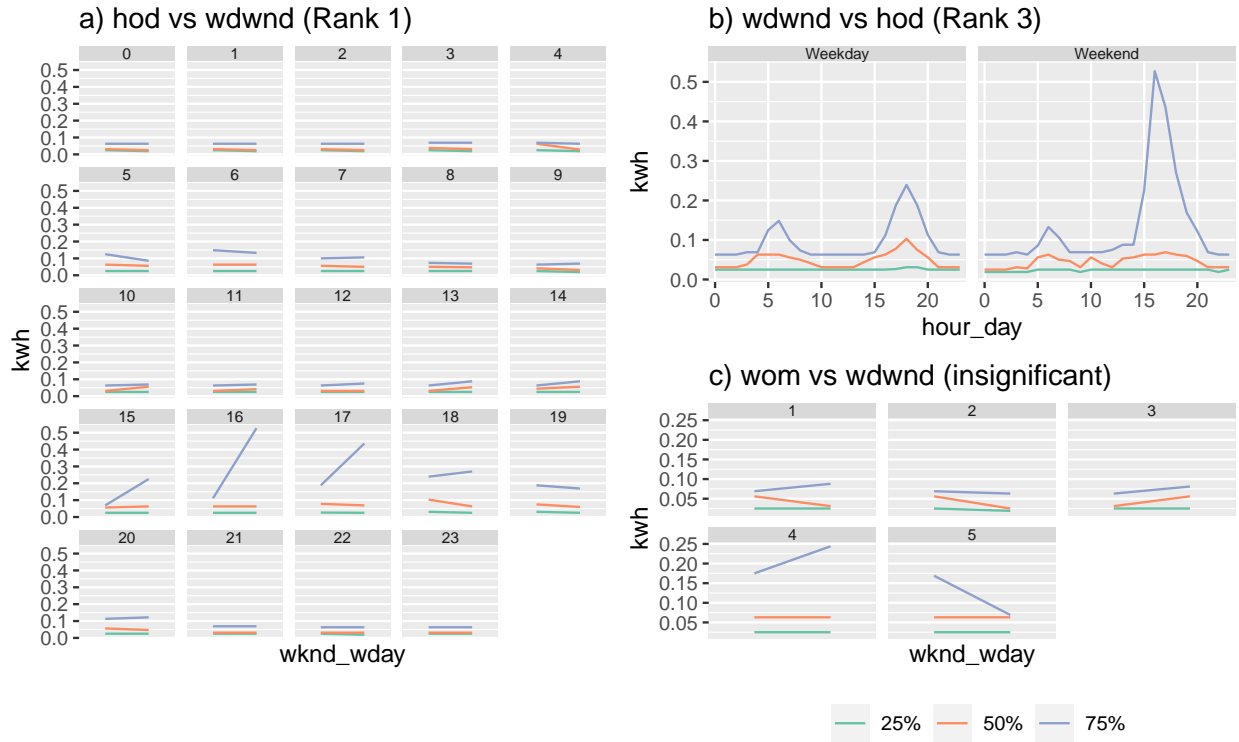


Figure 15: Distribution of energy demand shown for household id 1 across hod in x-axis and wd-wnd in facets in a) and just the reverse in b). In c), distribution of energy demand for household id:4 shown across hod and wd-wnd. It can be seen that the differences in distributions are more apparent when viewed in a) as compared to b). It seems like there is more difference in the distributions of hod for b) compared to c). This also confers with the value of the normalised measure shown in Figure 11.

of the week are also important (members are in academia and hence might have more flexible routines). The periodic pattern is very similar to id 8, which has a very different demographic property. Households id 2 and 3 are similar, in terms of linear display, periodic patterns as well as demographics. Different periodic behavior could be observed in households with very similar demographics (id 5 compared to 6 and 7 - only the variable profession is different) and similar periodic behavior can stem from households with very different demographics (id 7 and 8 - differs in all variables in 4). This could also be verified from the corresponding linear representation in 16(b).

Table 5: *Ranking of harmonies for the eight households with significance levels.*

facet variable	x variable	id 1	id 2	id 3	id 4	id 5	id 6	id 7	id 8
hod	wdwnd	1 ***	2 *	1 **	2 **	3	1 **	3	3 *
dom	hod	2 ***	4	3 **	3 **	4	3 *	4	6
wdwnd	hod	3 **	10	7	7	6	8	8	10
hod	wom	4	9	6	5	5	5	5	5
wom	wdwnd	5	14	14	10	12	9	12	13
hod	dow	6	1 ***	2 **	1 ***	1 *	2 **	2 **	1 **
wdwnd	wom	7	12	13	8	7	7	10	12
dow	hod	8	3	4 **	4 **	2	4 *	1 ***	2 **
hod	dom	9	7	10	13	10	10	9	4
wom	dow	10	6	8	9	8	6	7	9
dow	wom	11	5	9	11	11	12	6	7
wom	hod	12	8	5	6	9	11	11	8
dom	wdwnd	13	13	11	12	14	14	14	14
wdwnd	dom	14	11	12	14	13	13	13	11

6 Discussion

Exploratory data analysis involve many iterations of finding and summarizing patterns. With temporal data available at more and more finer scales, exploring periodicity has become over-

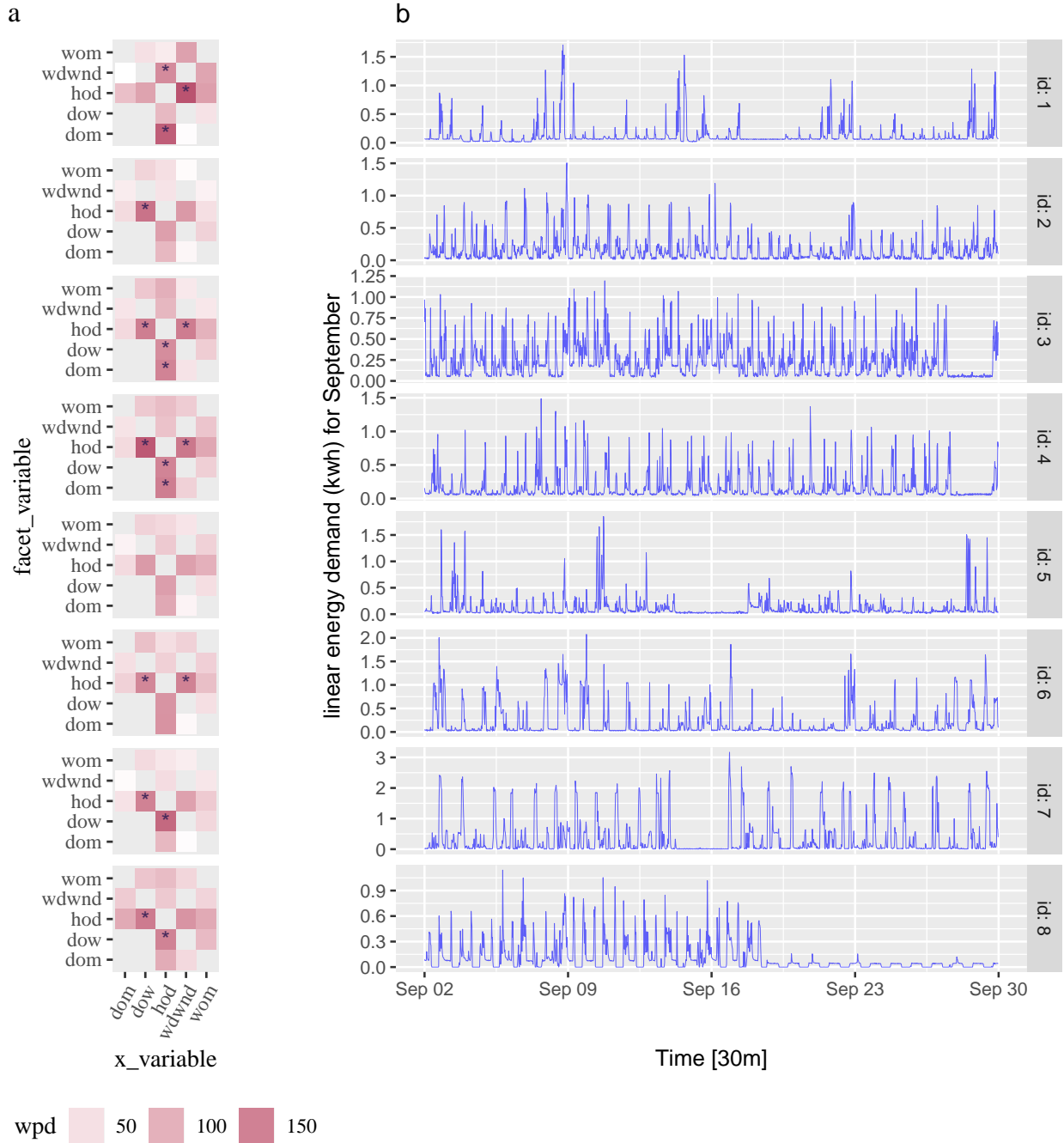


Figure 16: *Harmony pairs are shown for all household ids. The darker the colour, the higher the importance of the harmony. Also, the ones bordered red are selected with 90 percent significance level. Visualizing the pairs in this way helps us to see the important cyclic granularities along the x-axis and facet along with the information that which households should be analyzed together.*

whelming with so many possible granularities to explore. A common solution would be to zoom into “interesting” segments, but there is no way to know the “interesting” segments a priori. This work refines the search of periodic patterns by identifying those for which the differences between the displayed distributions is greatest, and rating them in order of importance for exploration.

A future direction of work could be to look at more individuals/subjects and group them according to similar periodic behavior. Behaviors across different harmonies would be varying for subjects and it would be hard to track the behavior when the number of individuals rise. One way to find groups would be to actually locate clusters who have similar periodic behavior.

References

- Bogner, K., Pappenberger, F. & Cloke, H. L. (2012), ‘Technical note: The normal quantile transformation and its application in a flood forecasting system’, *Hydrol. Earth Syst. Sci.* **16**(4), 1085–1094.
- Buja, A., Cook, D., Hofmann, H., Lawrence, M., Lee, E.-K., Swayne, D. F. & Wickham, H. (2009), ‘Statistical inference for exploratory data analysis and model diagnostics’, *Royal Society Philosophical Transactions A* **367**(1906), 4361–4383.
- Dang, T. N. & Wilkinson, L. (2014), ScagExplorer: Exploring scatterplots by their scagnostics, in ‘2014 IEEE Pacific Visualization Symposium’, pp. 73–80.
- Gupta, S., Hyndman, R. J., Cook, D. & Unwin, A. (2020), ‘Visualizing probability distributions across bivariate cyclic temporal granularities’.
- Hyndman, R. J. & Fan, Y. (1996), ‘Sample quantiles in statistical packages’, *Am. Stat.* **50**(4), 361–365.
- Hyndman, R. J., Liu, X. & Pinson, P. (2018), ‘Visualizing big energy data: Solutions for this crucial component of data analysis’, *IEEE Power and Energy Magazine* **16**(3), 18–25.
- Kullback, S. & Leibler, R. A. (1951), ‘On information and sufficiency’, *Ann. Math. Stat.* **22**(1), 79–86.

- Lin, J. (1991), ‘Divergence measures based on the shannon entropy’, *IEEE Transactions on Information Theory* **37**(1), 145–151.
- Majumder, M., Hofmann, H. & Cook, D. (2013), ‘Validation of visual statistical inference, applied to linear models’, *J. Am. Stat. Assoc.* **108**(503), 942–956.
- Menéndez, M. L., Pardo, J. A., Pardo, L. & Pardo, M. C. (1997), ‘The Jensen-Shannon divergence’, *J. Franklin Inst.* **334**(2), 307–318.
- R Core Team (2019), *R: A Language and Environment for Statistical Computing*, R Foundation for Statistical Computing, Vienna, Austria.
URL: <https://www.R-project.org/>
- Tukey, J. W. & Tukey, P. A. (1988), ‘Computer graphics and exploratory data analysis: An introduction’, *The Collected Works of John W. Tukey: Graphics: 1965-1985* **5**, 419.
- Wang, E., Cook, D. & Hyndman, R. J. (2020a), ‘Calendar-based graphics for visualizing people’s daily schedules’, *Journal of Computational and Graphical Statistics* . to appear.
- Wang, E., Cook, D. & Hyndman, R. J. (2020b), ‘A new tidy data structure to support exploration and modeling of temporal data’, *Journal of Computational and Graphical Statistics* . to appear.
- Wilkinson, L., Anand, A. & Grossman, R. (2005), Graph-theoretic scagnostics, in ‘IEEE Symposium on Information Visualization, 2005. INFOVIS 2005.’, IEEE, pp. 157–164.